CHIN. PHYS. LETT. Vol. 38, No. 7 (2021) 077103

Concurrent Structural and Electronic Phase Transitions in V_2O_3 Thin Films with Sharp Resistivity Change

Chuang Xie(谢闯)[1], Ling Hu(胡令)[2*], Ran-Ran Zhang(张冉冉)[3], Shun-Jin Zhu(朱顺进)[2], Min Zhu(朱敏)[2], Ren-Huai Wei(魏仁怀)[2], Xian-Wu Tang(汤现武)[2], Wen-Hai Song(宋文海)[2], Xue-Bin Zhu(朱雪斌)[2*], and Yu-Ping Sun(孙玉平)[2,3,4*]

[1]*Institutes of Physical Science and Information Technology, Anhui University, Hefei 230601, China*
[2]*Key Laboratory of Materials Physics, Institute of Solid State Physics, HFIPS, Chinese Academy of Sciences, Hefei 230031, China*
[3]*High Magnetic Field Laboratory, HFIPS, Chinese Academy of Sciences, Hefei 230031, China*
[4]*Collaborative Innovation Center of Advanced Microstructures, Nanjing 210093, China*

(Received 29 March 2021; accepted 8 May 2021; published online 3 July 2021)

The relationship between structural and electronic phase transitions in V_2O_3 thin films is of critical importance for understanding of the mechanism behind metal–insulator transition (MIT) and related technological applications. Despite being extensively studied, there are currently no clear consensus and picture of the relation between structural and electronic phase transitions so far. Using V_2O_3 thin films grown on r-plane Al_2O_3 substrates, which exhibit abrupt MIT and structural phase transition, we show that the electronic phase transition occurs concurrently with the structural phase transition as revealed by the electrical transport and Raman spectra measurements. Our result provides experimental evidence for clarifying this issue, which could form the basis of theoretical studies as well as technological applications in V_2O_3.

DOI: 10.1088/0256-307X/38/7/077103

Vanadium sesquioxide (V_2O_3) is an archetypical correlated oxide which exhibits a metal–insulator transition (MIT) accompanied by a structural phase transition (SPT) and a magnetic transition from a high-temperature paramagnetic metallic (PM) phase with a corundum structure to a low-temperature antiferromagnetic insulating (AFI) phase with a monoclinic structure around 160 K.[1] The entanglement of MIT with SPT and magnetic transition complicates the underlying physics and hinders a complete understanding of the MIT.[2–7] An important question is whether electronic correlation or structural effect accounts for the MIT in V_2O_3. Therefore, the clarification of the relation between SPT and MIT is a prerequisite to understand the mechanism behind these transitions. Despite decades of effort, clear consensus and a picture of the relation between SPT and MIT have not yet emerged.[1–10] Extended x-ray absorption fine structure (EXAFS) measurements have indicated that a continuous increase of the monoclinic distortion in the basal plane is observed far above the MIT.[2] Experimental evidence of the lattice precursor of the MIT has been revealed by surface acoustic waves in V_2O_3 thin films.[3] The MIT and SPT have been founded to decouple by a combining study of near-field infra-red (IR) imaging and x-ray diffraction (XRD) in V_2O_3 thin films.[4] In contrast, the MIT has been found to be tightly coupled to the SPT in V_2O_3 thin films by virtue of IR spectroscopy and XRD to determine electronic and structural phase fractions across the transition.[5] Furthermore, low-energy muon spin relaxation study has demonstrated that the magnetic transition occurs simultaneously with both MIT and SPT.[6]

Especially, Raman spectroscopy is a quick, convenient, non-destructive, and non-invasive probe for characterizing the SPT.[8–18] However, the Raman spectroscopy in V_2O_3 gives rise to controversial results regarding to the relation between SPT and MIT.[8–10] The Raman spectra in the V_2O_3 single crystal corresponding to phonon and magnon excitations exhibits drastic changes across the MIT, indicating the intertwined electronic, structural, and magnetic transitions.[8,9] However, decoupling of the MIT and SPT with a temperature interval of ∼23 K has been observed in a V_2O_3 thin film grown on a Si substrate by combining temperature-dependent Raman spectra and resistivity measurements.[10]

V_2O_3 thin films are sensitive to numerous factors such as strain states, substrate disorders, substrate orientations, and growth atmospheres, which account for the diverse electrical transport properties and much broadening MIT as compared to the bulk material.[10,19–25] The transition temperature of MIT

Supported by the National Key R&D Program of China (Grant No. 2017YFA0403600), and Joint Funds of the National Natural Science Foundation of China and the Chinese Academy of Sciences Large-Scale Scientific Facility (Grant No. U1532149).
*Corresponding authors. Email: huling@issp.ac.cn; xbzhu@issp.ac.cn; ypsun@issp.ac.cn
© 2021 Chinese Physical Society and IOP Publishing Ltd

($T_{\rm MIT}$) derived from the resistivity derivatives with peak values in V_2O_3 thin films represents the formation or destruction of percolation conduction.[4,10,26] As a result, the $T_{\rm MIT}$ would be sensitive to the change of local conducting paths. In contrast, the Raman spectra is volume sensitive.[8–18] The degree of decoupling between SPT and MIT may be overestimated in V_2O_3 thin films with broadening MIT.[3–6,10] In this respect, the realization of sharp MIT in V_2O_3 thin films would be the precondition for clarifying this issue and technological applications as well.[5,6,26–28]

A previous study has reported that V_2O_3 thin films grown on r-plane Al_2O_3 substrates are more prone to obtain sharp MIT than on the c-plane of Al_2O_3 substrates.[25] Furthermore, the variation of oxygen stoichiometry could strongly affect the electrical transport properties as well as MIT due to the multivalent nature of vanadium.[29–31] As a result, the MIT in V_2O_3 thin films would critically depend on the film growth conditions, which lead to the stabilization of specific vanadium oxides.[22,30,32–34] During growth of oxide films, the oxygen sources are the target, the background gas, and the substrate.[32,35,36] Therefore, precise control of growth atmosphere is vital to stabilize the +3 oxidation state of vanadium for the growth of V_2O_3 thin films when using either a metal target associated with oxidation or a V_2O_5 target associated with reduction.[22,30,37] In this respect, the V_2O_3 ceramic target may be a better choice for growth of stoichiometric V_2O_3 thin films.[19–21] The commonly used Al_2O_3 substrate can be regarded as having negligible oxygen contribution to the V_2O_3 thin film because of high formation energy of oxygen vacancy.[38] Based on the above considerations, we report the growth of V_2O_3 thin films on r-plane Al_2O_3 substrates by pulsed laser deposition (PLD) from a V_2O_3 ceramic target. Electrical transport measurements reveal that the V_2O_3 thin films deposited at substrate temperature ($T_{\rm S}$) of 773–923 K exhibit obvious MIT. In particular, the V_2O_3 thin film deposited at 923 K exhibits excellent MIT characteristics with sharp and large resistivity change. Raman spectroscopy investigation shows that the SPT related to the phonon modes of corundum and monoclinic structures occur concurrently with MIT.

V_2O_3 thin films of ∼70 nm were grown on r-plane Al_2O_3 substrates by PLD. A KrF excimer laser with a repetition rate of 5 Hz and an energy density of 2 J/cm^2 was focused on a V_2O_3 ceramic target. During film growth, the $T_{\rm S}$ was varied in the range of 773–923 K and the oxygen partial pressure in the growth chamber was maintained at $\sim 2 \times 10^{-4}$ Pa. Structural properties of the V_2O_3 thin films were characterized by XRD using Cu K_α radiation at room temperature. The film thickness was determined to be ∼70 nm by a field emission scanning electron microscope (Fig. S1 in the Supplementary Material). The chemical component and valence states of the elements were evaluated by x-ray photoelectron spectroscopy (XPS) with monochromatic Al K_α ($h\nu$ = 1486.6 eV). Binding energy data is referenced to the C 1s peak of 284.8 eV. Electrical transport properties were measured on a physics properties measurement system (PPMS) using the standard four-probe method setup. The Raman spectra measurements were performed from 25 K to 300 K by using a Horiba Jobin YvonT64000 Micro-Raman instrument with a torus 532 laser (λ = 532 nm) as an excitation source in a backscattering geometry. A back-illuminated charge coupled device (CCD) cooled by liquid nitrogen was used to detect the scattered light.

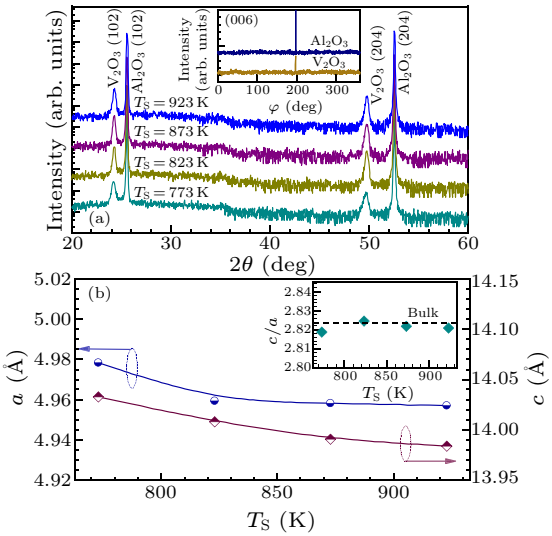

Fig. 1. (a) XRD θ–2θ profiles of V_2O_3 thin films grown on r-plane Al_2O_3 substrates at different $T_{\rm S}$. The inset shows the typical ϕ scan of the V_2O_3 thin film and Al_2O_3 substrate (006) reflections. (b) The change of a- and c-axis lattice parameters of V_2O_3 thin films with $T_{\rm S}$. The inset shows the variation of c/a ratio with $T_{\rm S}$. The dashed line indicates the c/a ratio of the V_2O_3 bulk material.

Figure 1(a) shows the XRD θ–2θ profiles of the V_2O_3 thin films grown on the r-plane Al_2O_3 substrate at different $T_{\rm S}$. It is clear that the V_2O_3 thin films exhibit oriented growth along the Al_2O_3 substrates without any secondary phases. The inset of Fig. 1(a) depicts the typical ϕ scan of the V_2O_3 thin film and Al_2O_3 substrate (006) reflections, which indicates the epitaxial growth of V_2O_3 thin films on r-plane Al_2O_3 substrates. The high quality of the V_2O_3 thin films can also be attested by the rocking curve measurements (ω-scan), exhibiting the full width at half maximum (FWHM) of 0.5°–0.6° (Fig. S2 in the Supplementary Material). The ratio of the mean size of crystalline domains in the vertical direction increases and saturates to half of the thickness with increasing $T_{\rm S}$ (Fig. S3 in the Supplementary Material). The c values of the V_2O_3 thin films were deduced from the (006)

asymmetric reflections. The a values of the V_2O_3 thin films were then determined from the interplanar spacing of the hexagonal based on the (102) reflections. As shown in Fig. 1(b), both a and c values of the V_2O_3 thin films weakly vary with increasing T_S. Specifically, the a (c) values decrease from 4.978 Å (14.033 Å) to 4.957 Å (13.984 Å) when the T_S is increased from 773 K to 923 K. As a consequence, c/a ratios of the V_2O_3 thin films range from 2.819 to 2.825, which is very close to that of the bulk material.[8] A previous study has stated that a values of V_2O_3 thin films grown on r-plane Al_2O_3 substrates close to the bulk value can be explained by considering the thermal expansion coefficient (TEC) of V_2O_3 and Al_2O_3.[25] The a-axis TEC of V_2O_3 and Al_2O_3 are $3.27 \times 10^{-5}\,K^{-1}$ and $7.30 \times 10^{-6}\,K^{-1}$, respectively.[39,40] The a-axis TEC mismatch between V_2O_3 and Al_2O_3 would expand the a-axis with increasing T_S. Therefore, the narrow distributions of a, c, and c/a values cannot be explained by the TEC mismatch and the reason needs further investigation.

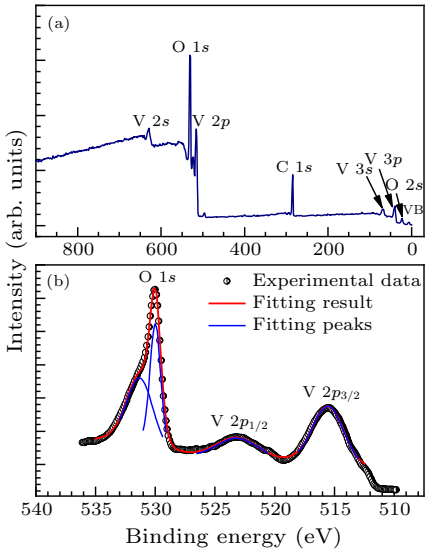

Fig. 2. (a) Typical XPS spectra for the V_2O_3 thin film of (a) wide scan and (b) V 2p and O 1s core levels.

XPS measurement has been performed to evaluate the chemical component and oxidation state of the V_2O_3 thin film. Figure 2(a) displays the typical wide scan spectrum of the V_2O_3 thin film. The elements V, O, and C can be clearly seen from the photoelectron peaks. The C 1s peak at 284.8 eV is taken as the binding energy reference. Figure 2(b) shows the spectra of the V 2p and O 1s core level, in which the dotted and solid lines represent the experimental data and fitting result. The fitting binding energies of V $2p_{3/2}$ and V $2p_{1/2}$ are 515.5 and 523.1 eV, which are consistent with the splitting of V 2p level into V $2p_{3/2}$ and V $2p_{1/2}$ due to spin-orbital coupling with a separated binding energy of ~7.6 eV. The corresponding line widths of full width at half maximum (FWHM) are 3.1 and 4.0 eV, respectively. These values are in good agreement with the previously reported values of +3 valence state in V_2O_3.[22,41,42] The O 1s level can be fitting to two peaks centered at 530 and 531.3 eV, which correspond to the V–O bound and the physically absorbed oxygen at the film surface, respectively.[22]

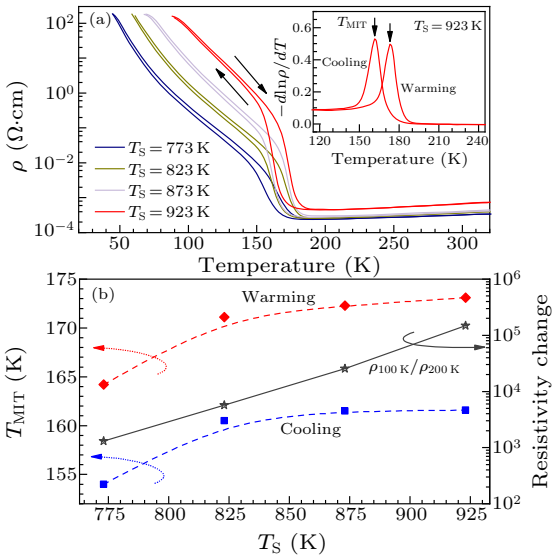

Fig. 3. (a) Temperature dependence of resistivity of V_2O_3 thin films grown on r-plane Al_2O_3 at different T_S. The inset shows the differential curve of resistivity with respect to temperature for the V_2O_3 thin film (T_S = 923 K). (b) The variation of transition temperature (T_{MIT}) and resistivity change ($\rho_{100\,K}/\rho_{200\,K}$) of the PM-AFI transition with the T_S.

Figure 3(a) shows the temperature-dependent resistivity for the V_2O_3 thin films deposited at different T_S. All the V_2O_3 thin films exhibit first-order MIT with obvious hysteresis between cooling and warming processes. Sakai *et al.* have indicated that the clamping of the V_2O_3 lattice by the r-plane substrate has less impact on the MIT due to the lesser restriction on simultaneous expansion of the a-axis and shrinkage of c-axis transition.[25] Kalcheim *et al.* have shown that a self-induced strain in a geometrically confined V_2O_3 thin film grown on a c-plane Al_2O_3 substrate manipulates the MIT.[43] Therefore, the lattices and MIT of the V_2O_3 thin films grown on r-plane Al_2O_3 substrates would have less of an affect by the substrates, which correspond to narrowly distributed c/a ratios [as shown in the inset of Fig. 1(b)]. This result can be understood by the scenario of trigonal distortion, in which the c/a ratio quantifies the degree of trigonal distortion to directly determine the PM-AFI transition.[44,45] It is clear that the trigonal distortion of VO_6 octahedra along (within) c-axis (ab plane) in the V_2O_3 thin films would be hardly affected when growing on the r-plane Al_2O_3 substrates. The MIT of V_2O_3 can be quantitatively characterized by the transition temperature (T_{MIT}), transition sharpness (ΔT), and resistivity change across

the transition.[4,10,26] The $T_{\rm MIT}$ is usually defined as the temperature where the resistivity derivatives exhibit a peak value. At $T_{\rm MIT}$, the sharpest change of resistivity represents the formation or destruction of percolation conduction.[4,26] The ΔT can be defined by the FWHW of the resistivity derivatives. It is clear that the transition sharpness (ΔT) of the V_2O_3 thin films can be remarkably enhanced (reduced) by increasing $T_{\rm S}$. As shown in the inset of Fig. 3(a), the V_2O_3 thin film deposited at 923 K has a ΔT of ∼10 K for both cooling and warming processes. Figure 3(b) depicts the variation of $T_{\rm MIT}$ and resistivity change across the transition ($\rho_{100\,\rm K}/\rho_{200\,\rm K}$) with the $T_{\rm S}$. The $T_{\rm MIT}$ exhibits slight increases towards V_2O_3 bulk materials with the increase of $T_{\rm S}$. Furthermore, the $\rho_{100\,\rm K}/\rho_{200\,\rm K}$ can be greatly improved more than 10^5 when the $T_{\rm S}$ is increased to 923 K. Therefore, the V_2O_3 thin film deposited at 923 K exhibits excellent MIT characteristics, which provides a very good platform for investigating the relationship between SPT and electronic transition in the V_2O_3 thin film.

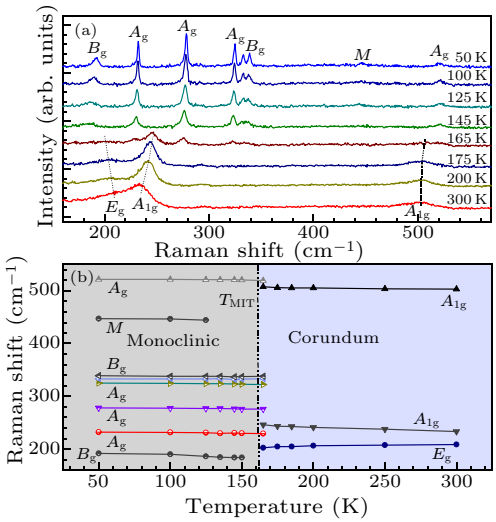

Fig. 4. (a) Temperature-dependent Raman spectra of the V_2O_3 thin film ($T_{\rm S}$ = 923 K) in the cooling process. (b) Raman shifts of the phonon modes as a function of temperature.

Figure 4(a) shows the temperature-dependent Raman spectra of the V_2O_3 thin film in the cooling process. The SPT occurs around the PM-AFI transition, which is clearly evident from the appearance of the phonon modes corresponding to the corundum and monoclinic structures (Fig. S4 in the Supplementary Material for the warming process). Figure 4(b) shows the Raman shift of phonon modes as a function of temperature. In the high temperature of V_2O_3, the corundum structure exhibits the symmetry of $R\bar{3}C$ space group and the D_{3d} point group two Raman irreducible representations $A_{1\rm g}$ and $E_{\rm g}$ modes.[46] At 300 K, the Raman peaks at ∼234 cm^{-1} and ∼502 cm^{-1} can be assigned to the $A_{1\rm g}$ modes, while the Raman peak at ∼208 cm^{-1} is of $E_{\rm g}$ mode (Fig. S5 in the Supplementary Material). The $A_{1\rm g}$ ($E_{\rm g}$) mode shifts to a high (low) frequency upon cooling from 300 K to 165 K (Fig. S6 in the Supplementary Material), which arises from the variation of the lattice structure.[1,47] In V_2O_3 with a corundum structure, the lattice vibrations related to $A_{1\rm g}$ and $E_{\rm g}$ modes strongly depend on lattice parameters, interionic distances, and elastic constants $C_{\mu\nu}$.[45,47,48] The space group of the low-temperature monoclinic structure changes to $B2/b$ with the C_{2h} point group, which has two groups of Raman active modes of A_g and $B_{\rm g}$ modes.[47] The Raman peaks locate at ∼230 cm^{-1}, 278 cm^{-1}, 324 cm^{-1}, and 520 cm^{-1} are of the $A_{\rm g}$ modes. The Raman locates at ∼192 cm^{-1}, ∼332 cm^{-1}, and ∼338 cm^{-1} can be assigned to the $B_{\rm g}$ phonon modes. The Raman peak at ∼448 cm^{-1} corresponds to a magnon scattering in the antiferromagnetic phase. It is clear that the corundum and monoclinic structures coexist in the hysteresis region at 165 K.

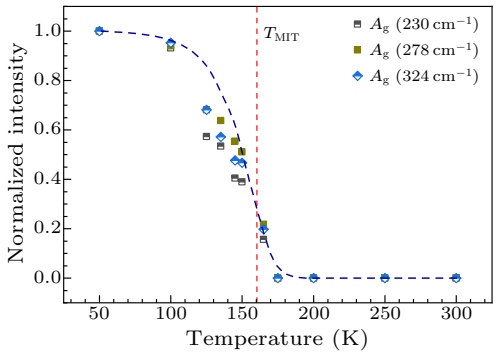

Fig. 5. Normalized intensity of $A_{\rm g}$ phonon mode at ∼230 cm^{-1}, ∼278 cm^{-1}, and ∼324 cm^{-1} in the V_2O_3 thin film versus temperature. The dotted lines are of guides for the eyes.

Figure 5 depicts the variation of the normalized intensity of the $A_{\rm g}$ phonon modes at ∼230 cm^{-1}, ∼278 cm^{-1}, and ∼324 cm^{-1} with temperature, which is normalized to that at 50 K in the AFI phase with a monoclinic structure. The three Raman phonon modes are chosen because they are at the position where the strongest Raman peaks of the monoclinic structure are. In the high-temperature PM phase with a corundum structure, the normalized intensity of the $A_{\rm g}$ phonon modes is equal to zero. The monoclinic phase begins to nucleate and grow when decreasing temperature, which is evidenced by the appearance of the $A_{\rm g}$ phonon modes. The intensities of the $A_{\rm g}$ phonon modes increase rapidly and saturate with further decreasing temperature, which are in good agreement with the resistivity change across the MIT. The similar phenomenon is also observed in the warming process (Fig. S7 in the Supplementary Material). A previous study has shown that the growth of insulating (metallic) domains in an metallic (insulating)

background on cooling (warming) in the percolation conduction of V_2O_3 thin film for the MIT tends to be along specific direction with respect to the Al_2O_3 substrate.[4] In contrast, the percolation conduction in the V_2O_3 thin film grown on the Si substrate may start with random growth of insulating (metallic) domains, which results in the lower T_{MIT} and broadening MIT. Therefore, the decoupling of SPT and MIT in the V_2O_3 thin film grown on a Si substrate may be extrinsic arising from the asynchronous contributions to electrical transport and Raman spectra by the coexistence and competition of the PM phase with a corundum structure and AFI phase with a monoclinic structure.[10] In our case, the growth of insulating (metallic) domains in the V_2O_3 thin film grown on an r-plane Al_2O_3 substrate could contribute to both electrical transport and Raman spectra in a synchronous manner, which results in the concurrent SPT and MIT.

In summary, the V_2O_3 thin films have been grown on r-plane Al_2O_3 substrates by PLD from a V_2O_3 ceramic target. The V_2O_3 thin film deposited at 923 K exhibits excellent MIT characteristics including $\Delta T \sim 10$ K and $\rho_{100\,K}/\rho_{200\,K} \sim 10^5$. Furthermore, temperature-dependent electrical transport and Raman spectra measurements reveal that the SPT and MIT occur concurrently in the V_2O_3 thin film with sharp resistivity change. Our result provides experimental evidence for understanding the mechanism behind the MIT in V_2O_3.

One can see the Supplementary Material for the cross-section SEM image, the rocking curve measurements (ω-scan), the variation of mean size of the crystalline domains, the decomposition of E_g and A_{1g} modes using Lorentzian fitting, the enlarged view of Raman spectra at different temperatures (300–165 K), the temperature-dependent Raman spectra of the V_2O_3 thin film ($T_S = 923$ K) and the normalized intensity of the A_g phonon mode at $\sim$230 cm^{-1}, $\sim$278 cm^{-1}, and $\sim$324 cm^{-1} in the warming process.

References

[1] McWhan D B and Remeika J P 1970 *Phys. Rev. B* **2** 3734
[2] Pfalzer P, Obermeier G, Klemm M, Horn S and denBoer M L 2006 *Phys. Rev. B* **73** 144106
[3] Kündel J, Pontiller P, Müller C, Obermeier G, Liu Z, Nateprov A A, Hörner A, Wixforth A, Horn S and Tidecks R 2013 *Appl. Phys. Lett.* **102** 101904
[4] McLeod A S, Heumen E V, Ramirez J G, Wang S, Saerbeck T, Guenon S, Goldflam M, Anderegg L, Kelly P, Mueller A, Liu M K, Schuller I K and Basov D N 2017 *Nat. Phys.* **13** 80
[5] Kalcheim Y, Butakov N, Vargas N M, Lee M H, del V J, Trastoy J, Salev P, Schuller J and Schuller I K 2019 *Phys. Rev. Lett.* **122** 057601
[6] Frandsen B A, Kalcheim Y, Valmianski I, McLeod A S, Guguchia Z, Cheung S C, Hallas A M, Wilson M N, Cai Y, Luke G M, Salman Z, Suter A, Prokscha T, Murakami T, Kageyama H, Basov D N, Schuller I K and Uemura Y J 2019 *Phys. Rev. B* **100** 235136
[7] Hansmann P, Toschi A, Sangiovanni G, Saha-Dasgupta T, Lupi S, Marsi M and Held K 2013 *Phys. Status Solidi B* **250** 1251
[8] Kuroda N and Fan H Y 1977 *Phys. Rev. B* **16** 5003
[9] Misochko O V, Tani M, Sakai K, Kisoda K, Nakashima S, Andreev V N and Chudnovsky F A 1998 *Phys. Rev. B* **58** 12789
[10] Majid S S, Shukla D K, Rahman F, Gautam K, Choudhary R J, Sathe V G and Phase D M 2017 *Appl. Phys. Lett.* **110** 173101
[11] Gasparov L V, Tanner D B, Romero D B, Berger H, Margaritondo G and Forro L 2000 *Phys. Rev. B* **62** 7939
[12] Kim H T, Chae B G, Youn D H, Maeng S L, Kim G, Kang K Y and Lim Y S 2004 *New J. Phys.* **6** 52
[13] Zhang S, Chou J Y and Lauhon L J 2009 *Nano Lett.* **9** 4527
[14] Chi Z H, Zhao X M, Zhang H, Goncharov A F, Lobanov S S, Kagayama T, Sakata M and Chen X J 2014 *Phys. Rev. Lett.* **113** 036802
[15] Saito R, Tatsumi Y, Huang S, Ling X and Dresselhaus M S 2016 *J. Phys.: Condens. Matter* **28** 353002
[16] Wang Y, Xiao J, Zhu H, Li Y, Alsaid Y, Fong K Y, Zhou Y, Wang S, Wu S, Wang Y, Zettl A, Reed E J and Zhang X 2017 *Nature* **550** 487
[17] Lee D, Chung B, Shi Y, Kim G Y, Campbell N, Xue F, Song K, Choi S Y, Podkaminer J, Kim T, Ryan P J, Kim J W, Paudel T R, Kang J H, Spinuzzi J W, Tenne D A, Tsymbal E Y, Rzchowski M S, Chen L Q, Lee J and Eom C B 2018 *Science* **362** 1037
[18] Gao J J, Si J G, Luo X, Yan J, Chen F C, Lin G T, Hu L, Zhang R R, Tong P, Song W H, Zhu X B, Lu W J and Sun Y P 2018 *Phys. Rev. B* **98** 224104
[19] Yonezawa S, Muraoka Y, Ueda Y and Hiroi Z 2004 *Solid State Commun.* **129** 245
[20] Allimi B S, Alpay S P, Goberman D, Huang T, Budnick J I, Pease D M and Frenkel A I 2007 *J. Mater. Res.* **22** 2825
[21] Allimi B S, Aindow M and Alpay S P 2008 *Appl. Phys. Lett.* **93** 112109
[22] Laurent S A, Mercey B, Chippaux D, Limelette P and Ch S 2006 *Phys. Rev. B* **74** 195109
[23] Brockman J, Samant M G, Roche K P and Parkin S S 2012 *Appl. Phys. Lett.* **101** 051606
[24] Dillemans L, Smets T, Lieten R R, Menghini M, Su C Y and Locquet J P 2014 *Appl. Phys. Lett.* **104** 071902
[25] Sakai J, Limelette P and Funakubo H 2015 *Appl. Phys. Lett.* **107** 241901
[26] Salev P, del V J, Kalcheim Y and Schuller I K 2019 *Proc. Natl. Acad. Sci. USA* **116** 8798
[27] Kalcheim Y, Camjayi A, del V J, Salev P, Rozenberg M and Schuller I K 2020 *Nat. Commun.* **11** 2985
[28] Yang Z, Ko C and Ramanathan S 2011 *Annu. Rev. Mater. Res.* **41** 337
[29] Ueda Y, Kosuge K and Kachi S 1980 *J. Solid State Chem.* **31** 171
[30] Thorsteinsson E B, Shayestehaminzadeh S and Arnalds U B 2018 *Appl. Phys. Lett.* **112** 161902
[31] Trastoy J, Kalcheim Y, del V J, Valmianski I and Schuller I K 2018 *J. Mater. Sci.* **53** 9131
[32] Hu L, Luo X, Zhang K J, Tang X W, Zu L, Kan X C, Chen L, Zhu X B, Song W H, Dai J M and Sun Y P 2014 *Appl. Phys. Lett.* **105** 111607
[33] Lee S, Meyer T L, Park S, Egami T and Lee H N 2014 *Appl. Phys. Lett.* **105** 223515
[34] Choi S, Son J, Oh J, Lee J, Jang J H and Lee S 2019 *Phys. Rev. Mater.* **3** 063401
[35] Schneider C W, Esposito M, Marozau I, Conder K, Doebeli M, Hu Y, Mallepell M, Wokaun A and Lippert T 2010 *Appl. Phys. Lett.* **97** 192107
[36] Stender D, Cook S, Kilner J A, Döbeli M, Conder K, Lip-

pert T and Wokaun A 2013 *Solid State Ionics* **249** 56
[37] Sakai J, Bavencoffe M, Negulescu B, Limelette P, Wolfman J, Tateyama A and Funakubo H 2019 *J. Appl. Phys.* **125** 115102
[38] Tanaka I, Oba F, Tatsumi K, Kunisu M, Nakano M and Adachi H 2002 *Mater. Trans.* **43** 1426
[39] Eckert L J and Bradt R C 1973 *J. Appl. Phys.* **44** 3470
[40] Yim W M and Paff R J 1974 *J. Appl. Phys.* **45** 1456
[41] Hryha E, Rutqvist E and Nyborg L 2012 *Surf. Interface Anal.* **44** 1022
[42] Liu X B, Lu H B, He M, Jin K J and Yang G Z 2014 *Sci. Chin.-Phys. Mech. Astron.* **57** 1866
[43] Kalcheim Y, Adda C, Salev P, Lee M, Ghazikhanian N, Vargas N M, del V J and Schuller I K 2020 *Adv. Funct. Mater.* **30** 202005939
[44] Muller O, Urbach J P, Goering E, Weber T, Barth R, Schuler H, Klemm M, Horn S and denBoer M L 1997 *Phys. Rev. B* **56** 15056
[45] Hu L, Xie C, Zhu S J, Zhu M, Wei R H, Tang X W, Lu W J, Song W H, Dai J M, Zhang R R, Zhang C J, Zhu X B and Sun Y P 2021 *Phys. Rev. B* **103** 085119
[46] Cowley E R 1969 *Can. J. Phys.* **47** 1381
[47] Tatsuyama C and Fan H Y 1980 *Phys. Rev. B* **21** 2977
[48] Yang H and Sladek R J 1985 *Phys. Rev. B* **32** 6634

Supplementary Material for "Concurrent Structural and Electronic Phase Transitions in V_2O_3 Thin Films with Sharp Resistivity Change"

Chuang Xie(谢闯)[1], Ling Hu(胡令)[2*], Ran-Ran Zhang(张冉冉)[3], Shun-Jin Zhu(朱顺进)[2], Min Zhu(朱敏)[2], Ren-Huai Wei(魏仁怀)[2], Xian-Wu Tang(汤现武)[2], Wen-Hai Song(宋文海)[2], Xue-Bin Zhu(朱雪斌)[2*], and Yu-Ping Sun(孙玉平)[2,3,4*]

[1]*Institutes of Physical Science and Information Technology, Anhui University, Hefei, 230601, China*

[2]*Key Laboratory of Materials Physics, Institute of Solid State Physics, HFIPS, Chinese Academy of Sciences, Hefei 230031, People's Republic of China*

[3]*High Magnetic Field Laboratory, HFIPS, Chinese Academy of Sciences, Hefei 230031, People's Republic of China*

[4]*Collaborative Innovation Center of Advanced Microstructures, Nanjing University, Nanjing 210093, People's Republic of China*

Corresponding author: huling@issp.ac.cn; **xbzhu@issp.ac.cn; ypsun@issp.ac.cn;**

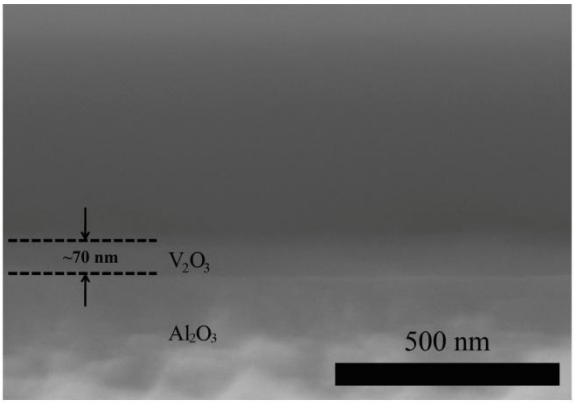

Fig. S1. Cross-section SEM image of V_2O_3 thin film grown on *r*-plane Al_2O_3 substrate.

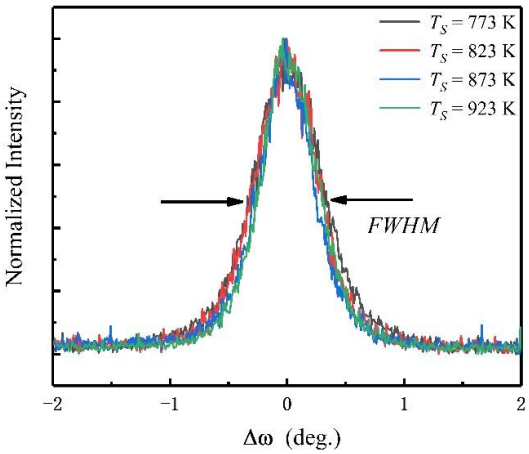

Fig. S2. Rocking curve around the (012) peak for the V_2O_3 thin films.

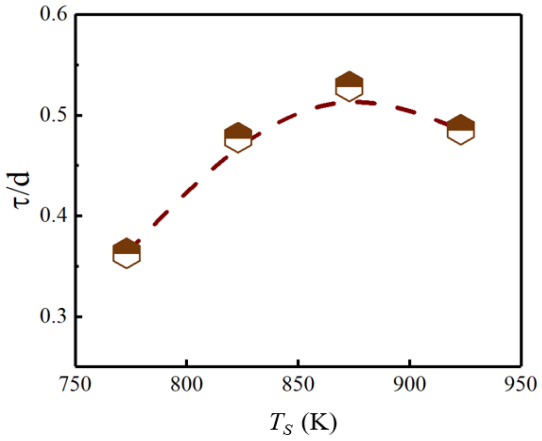

Fig. S3. Ratio of the mean size of the crystalline domains in the vertical direction, τ, to the V_2O_3 film thickness as a function of T_S. The values of τ were determined from the FWHM of the V_2O_3 (012) peak using Scherrer formula.

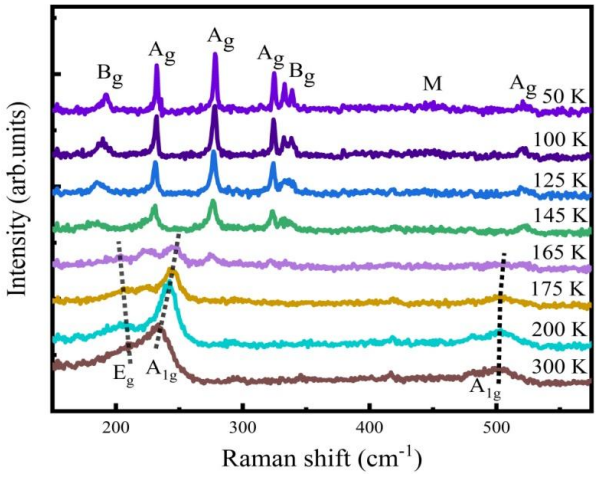

Fig. S4. Temperature dependent Raman spectra of the V_2O_3 thin film (T_S = 923 K) in the warming process.

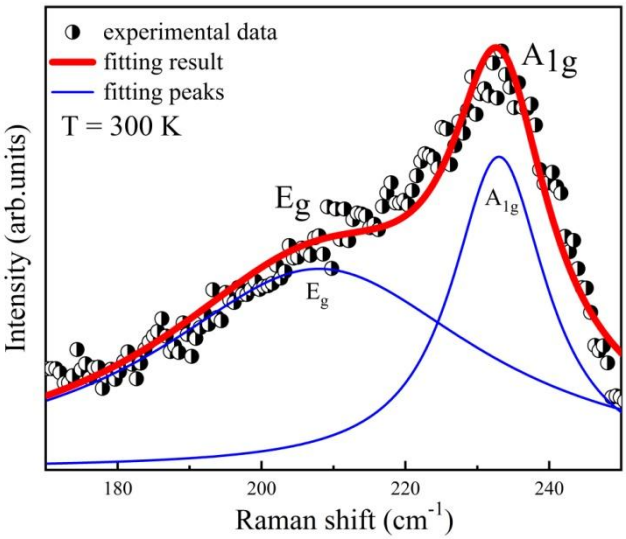

Fig. S5. The decomposition of E_g and A_{1g} modes using Lorentzian fitting.

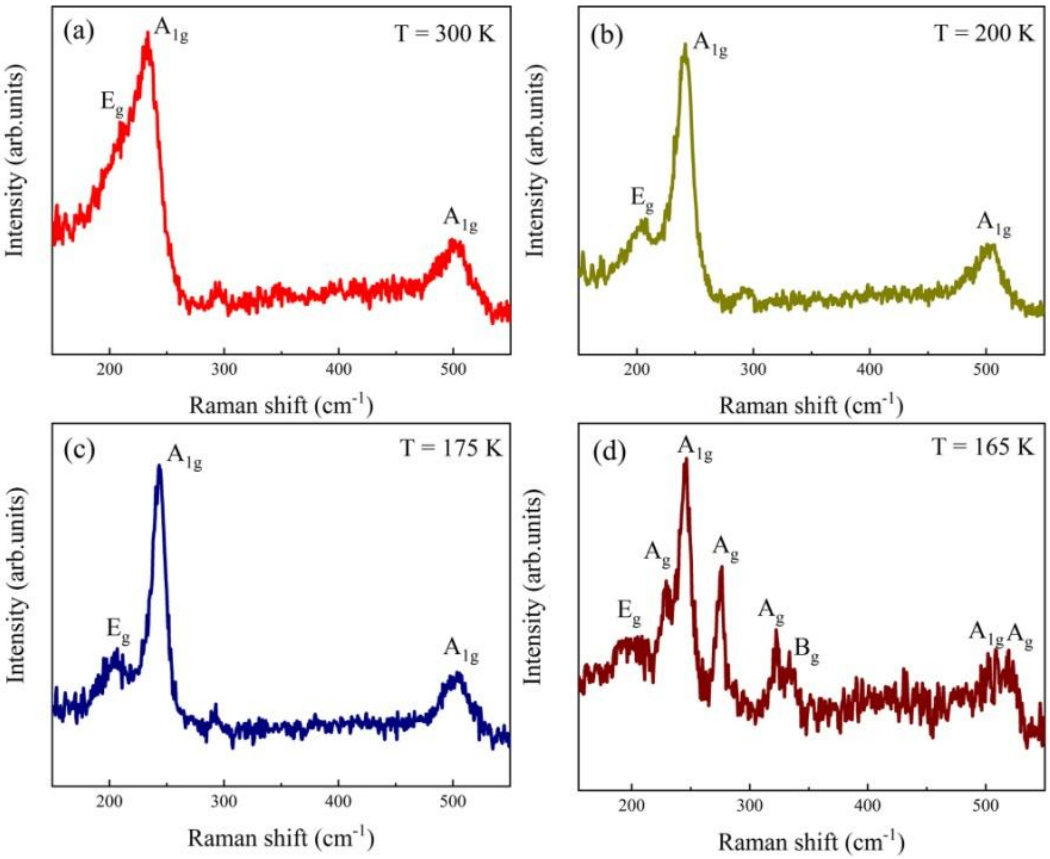

Fig. S6. The enlarged view of Raman spectra at different temperatures.

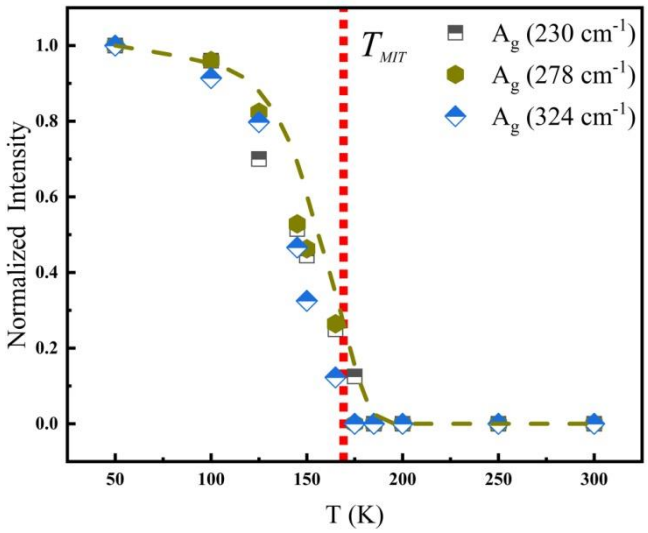

Fig. S7. Normalized intensity of A_g phonon mode at ~230 cm^{-1}, ~278 cm^{-1}, and ~324 cm^{-1} in the V_2O_3 thin film as a function of temperature in the warming process. The dotted lines are guides for the eyes.